eman ta zabal zazu

Universidad del País Vasco   Euskal Herriko Unibertsitatea

Facultad de Medicina y Enfermería
Departamento de Medicina y Cirugía

Nasal cartilage regeneration by procondrogenic 3D bio-printed structure: a strategy to improve regeneration.

TESIS DOCTORAL
Carlos Miguel Chiesa Estomba
Noviembre, 2021

(dedicatoria)

Me gustaría dedicar esta tesis a mi Esposa Angelica y a mi familia por siempre apoyarme en mis inquietudes científicas. A mis amigos y compañeros Frank, Alejandra, Jose Angel, Alex y Ekhiñe asi como a mi jefe y tutor Xavier Altuna por creer en mi y apoyarme.

A Ana, Ander, Raquel, Claudia, al resto del equipo en la unidad multidisciplinar de impresión 3D del instituto biodonostia, a Carlos, Eli y el resto de los compañeros del animalario (Biodonostia).

A mis amigos y al resto de compañeros de trabajo.

ÍNDICES

INDEX

TABLES **Page**

FIGURES.   **Page**

ACRONYMS:

ECM	Extracellular matrix
GFs	Growth factors
SLA	Stereolithography
UV	Ultraviolet
FFF	Fused filament fabrication
FDM	Fused deposition modeling
SLS	Selective laser sintering
MSCs	Mesenchymal stem cells
GAG	Glycosaminoglycans
ASCs	Adipose-derived stromal cells
PCL	Polycaprolactone
PSI	Pounds per square inch
Mm	Millimeter.
Seg	Seconds
P/S	Penicillin/Streptomycin
μm	Micrometre
RPM	Revolutions per minute.
CO_2	Carbon dioxide
ITS	Insulin-Transferrin-Selenium
ML	Mililiter.
PBS	Phosphate buffered saline
DNA	Desoxyribonucleic acid.
RNA	Ribonucleic acid
Ng	Nanogram

Col   Collagen

SOX   Cyclooxygenase

ACAN   Aggrecan - cartilage-specific proteoglycan core protein

GAPDH   Glyceraldehyde 3-phosphate dehydrogenase

SEM   Scanning electron microscopy

PCR   Polymerase chain reaction

1. INTRODUCTION

INTRODUCTION

Three-dimensional (3D) printing technology was first introduced in 1986 by Charles W. Hull,[1] who originally named it as stereolithography or additive manufacturing. Over the last two decades, despite a relevant gap in its widespread adoption, this technology has acquired a significant reputation and is being prevalently used at the research and manufacturing levels in several fields.[2-4] More recently, diverse medical sub-specialties have started considering novel 3D bioprinting approaches, based on the concept of combining living cells and biomaterials, controlling cell proliferation, attachment, and migration within 3D printed scaffolds. Although still far from clinical use, these techniques could represent an initial step to create complex organs.

9.1. The surgical and tissular issue

The nasal cartilage represents a specialized connective tissue devoid of the nerves, blood vessels, and lymphatic vessels. This tissue presents unique challenges for tissue engineering as it has relatively low cellularity (composed of approximately 1% chondrocytes and 99% extracellular matrix [ECM]), specific mechanical characteristics, and a low intrinsic self-repair capacity.[5,6]

Nasal defects that affect the craniofacial composition may arise from several etiologies, such as congenital malformation or cartilage absence, iatrogenic secondary to functional, oncological resection, or trauma. Importantly, nasal defects are related to both cosmetic and functional deficits.[7] Currently, treatment is based on reconstruction with local flaps or autologous cartilage grafts. However, these techniques are associated with increased donor-site morbidity, and the amount of tissue obtained is limited in size and shape depending on the availability of donor tissue. Thus, alternative techniques that take into consideration the complexity related to the anatomical 3D geometry are essential for the treatment of these pathologies.

Historically, the lack of autologous cartilage analogues for nasal reconstruction has led surgeons to try and develop a variety of allogeneic and synthetic grafts, which

have thus far failed to replace the current gold standard. The efficacy of each material tested and their associated complications, such as extrusion, risk of infection, and foreign body reaction, are well described in the literature.[8,9] Moreover, allogeneic grafts can be affected by immune rejection and have an associated risk of disease transmission.[8,9]

A currently used alternative option for autologous rib reconstruction is the use of prefabricated, synthetic implant, MedPor (Stryker Corporation, Kalamazoo, Michigan, USA), or porous, high-density polyethylene implants.[10] The benefits of this technique include avoiding donor-site morbidity from autologous cartilage harvesting and lower variability with the framework appearance, bypassing the technically demanding carving of the framework. However, personalized frameworks are not available for patient-specific anatomical defects. Although MedPor is approved by the Food and Drug Administration, it has a greater incidence of framework extrusion and soft tissue necrosis when compared to autologous cartilage reconstruction.[11]

9.2. The 3D bioprinting paradigm

In recent years, biomedical scaffolds made of natural or synthetic polymers have emerged from the biomedical and tissue engineering fields as a potential tool for nasal cartilage repair[12,13] owing to their ability to replace or functionally and structurally regenerate native tissues. A scaffold has the following functions: it should provide internal pathways for cell attachment, differentiation, and migration; it must permit trafficking of various growth factors (GFs) and waste products; it should maintain its shape when the cells are growing, whilst being permissive to partial remodeling; and it should have adequate mechanical properties.[14] Ideally, the scaffold manufacturing process should be individually calibrated to achieve these functions, modifying the porosity (pore size distribution, pore volume, and pore interconnectivity) of scaffolds to increase cell affinity, proliferation, migration, attachment, and differentiation, and even enable nutrient and oxygen transport in a purpose-built manner.[15,16]

All these advantages have increased the interest of scientists in the application of scaffolds with well-designed and specific architectures that can efficiently provide a

native niche for cells in *ex-vivo/in-vitro* environments and in animal and human models.[17,18] Generally, the ECM is composed of a 3D ultrafine fibrous architecture with certain physical and mechanical properties that are specific to each tissue in the body. Concurrently, ECM modulates cell morphology and functions, such as adhesion, proliferation, and differentiation.[19] Therefore, scaffolding strategies should consider these essential properties during the design and fabrication process.

9.3. Types of 3D-Printing methods useful in biomedical apllications

1.3.1. Vat Photopolymerisation Method

The vat photopolymerisation process was patented in 1986 by Charles W. Hull.[1] The stereolithography (SLA) machine uses UV light to create 3D structures and is based on the vat photopolymerisation principle that monomer resins are photosensitive when exposed to UV light or another similar power source. Photopolymerisation is driven by a chemical reaction that produces free radicals when exposed to certain wavelengths of light. Photons from the light source dissociate the photoinitiator to a high energy radical state and the free radicals induce the polymerisation of the macromer or monomer solution. However, the problem with this photopolymerisation process is that the created free radicals can cause damage to cell membrane, proteins, and nucleic acids. To combat this, hydrogel scaffolds using this technology have been created recently using 3D printing.[20]

1.3.2. Fused Filament Fabrication Method

Fused filament fabrication (FFF) or fused deposition modeling (FDM) printers use a thermoplastic filament; during the process the filament is heated to its melting point and then extruded to prepare a 3D structure. Thermoplastic filaments are extruded onto the substrate to fabricate a 3D structure. All the procedures are controlled by a computer that translates the dimensions of a structure into X, Y, and Z co-ordinates during printing. This technique is a good and reliable option for fabricating 3D scaffolds in tissue engineering applications and many researchers have reported using this method for tissue engineering. The advantages of this method in tissue

engineering applications are ease of use, the variety of biomaterials, good mechanical properties, and that a solvent is not required. The disadvantages are material restriction related to thermoplastic polymers and the lack of guarantee that that it can be printed with cells effectively due to the high manufacturing temperature.[20]

1.3.3. Selective Laser Sintering Method

The selective laser sintering (SLS) technique uses a laser as a power source to form solid 3D structures, using a high-powered laser for powder sintering to form a scaffold. This method utilises selective laser printing from 3D modelling software on the surface of a powder bed and may print using several different materials, such as ceramics, metals, and polymers. This technology can be used for tissue engineering, creating different scaffold structures from polymeric biomaterials and their composites, like bone.[21] These composite scaffolds are effective at supporting cell adhesion, proliferation, and growth, but have met with limited success in terms of accurately achieving the required porosity levels.[22] Other authors have reported a technique to design and manufacture a customised titanium mesh for minimal bone augmentation of an atrophic maxillary arch, guided by the final position of the prosthesis and according to the implants necessary for its support.[23] The main advantage of this process for tissue engineering applications is the wide range of biomaterials that can be used. The disadvantage of laser printers is that they tend to be large, cumbersome, and expensive.

1.3.4. Inkjet 3D Printing

Inkjet bioprinters are the most used type of printer for biological and non-biological applications. This method creates different structures using a rapid prototyping and layered manufacturing technology and has seen significant developments in the use of polymeric bioink printing for applications in biological and tissue engineering fields. Different kinds of tissue can be created using printable hydrogels, such as retinal tissue and adipose tissue matrix, among others. The advantages of inkjet 3D bioprinting for tissue engineering applications are patient-customised fabrication, rapid production, the low cost of production, and ease of incorporating both the drug and biomolecules.

In addition, it can be printed with the cells. The main disadvantages are the size limitations, biomaterials available, low resolution, and that it has the worst mechanical properties.[20]

Types of 3D-Printing methods
a) Vat Photopolymerisation Method
b) Fused Filament Fabrication Method
c) Selective Laser Sintering Method
d) Inkjet 3D Printing

Table 1. Types of 3D-Printing methods useful in biomedical apllications.

9.4.   The Cellular situation

As mentioned above, scaffolds are intended to support cell growth and environmental equilibrium. Hence, ECM secretion is a critical stage during chondrocyte maturation. This phenomenon was detected via observation of ECM-like structures on stem cell-seeded scaffolds after chondrogenic induction.[24] Among the various proteins present in the ECM, type II collagen is the major component of hyaline-like cartilage.[25,26] Nasal cartilage is composed of hyaline cartilage, which consists of densely packed collagen and proteoglycan-based ECM embedded with chondrocytes.[27] Moreover, it is a relatively simple structure with mechanically robust and elastic properties, compared with other tissues in the body. These characteristics justify a concerted effort to replicate this type of tissue.[28]

One of the main problems in translating this technology from the laboratory to surgical or clinical facilities is the need for sourcing autologous chondrocytes. However, some solutions are on the horizon. Ear, nose, and throat surgeons usually perform septal surgeries. They represent an opportunity for harvesting the nasal cartilage through an easy and low-invasive surgery, with reduced morbidity.[29]

Human nasal chondrocytes proliferate approximately four times faster than human articular chondrocytes in monolayer culture and have markedly higher chondrogenic capacity in *in-vitro* tissue-engineered constructs.[30] In addition, nasal chondrocytes exhibit a higher proliferation and chondrogenic capacity than articular chondrocytes.[31]

Chondrocytes induce chondrogenic differentiation of mesenchymal stem cells (MSCs) via the production of exogenous GFs such as cytokine-like protein 1, bone morphogenetic protein-2, parathyroid hormone-related peptide, transforming growth factor-beta, paracrine, juxtacrine, and gap-junction signaling pathways.[32-35] In this way, chondrocytes provide the chondrogenic niche required for the commitment of MSCs to the chondrogenic phenotype, circumventing the need for exogenous GF delivery. Additionally, chondrocytes provide a matrix for MSC migration and prevent ossification of MSC-derived chondrocytes.[36]

The limitation of using chondrocytes solely for cartilage tissue engineering is the large number of cells needed to seed human-sized craniofacial frameworks.[37-41] The number of chondrocytes available from autologous cartilage is limited, and passaging chondrocytes induce dedifferentiation with loss of type II collagen and glycosaminoglycan (GAG) production.[42,43] MSCs, of which ample cell quantities are available, have been posited as a solution to seeding requirements. Various MSC types, including adipose-derived stromal cells (ASCs) and bone marrow stromal cells, are capable of chondrogenic differentiation.[44,45] However, the chondrogenic commitment of MSCs requires exogenous delivery of GFs for weeks, and cells can demonstrate a propensity for ossification.[46,47] In addition, neovascularization surrounding 3D tissue-engineered cartilaginous constructs has proven to be a challenge for the long-term stability of these constructs, particularly with the fragility of ASCs in hypoxic tissue environments.[48]

Another relevant factor regarding the histological characteristics of the scaffold is the evaluation of cellular proliferation. In the indexed literature, only Apelgren *et al.*

described chondrocyte proliferation quantitatively in bioprinted chondrocytes as well as confirms the boosting effect of co-culture with MSCs.[49]

9.5. Reserch perspective

In recent years, 3D printing of tissue-engineered cartilaginous scaffolds is intended to close this gap and provide bioprinted tissue designed to fit the specific geometric and functional requirements of each defect, avoiding donor-site morbidity and personalizing therapy that best responds to patient needs. To achieve this goal, it is necessary to consider some criteria, such as the size, shape, and mechanical properties of the nasal cartilage.[50] The main goal of any tissue engineering strategy is to replicate such conditions and provide an engineered construct as similar as possible to the native tissue.

In this study, we described the use of 3D-Bioprinting to create a nasal septal cartilage model from rabbit chondrocytes, analyzing the in-vitro and in-vivo behavior, the mechanical properties as well as quantitation of the chondrogenic potential of the chondrocytes in 3D-bioprinted constructs implanted into rabbit.

2. HYPOTHESIS

1. HYPOTESIS

The idea to provide a bio-printed tissue designed to fit the specific geometric and functional requirements of each cartilage defect, avoiding donor-site morbidity, and personalizing the type of therapy represents one the most amazing fields in medicine and bioengineering. However, to achieve this goal it is necessary to consider some criteria, such as the size, shape, biological and mechanical properties of the cartilage.[50] Nowadays, the use of a co-culture method, for which chondrocytes and growth factors are simultaneously seeded into tissue engineering scaffolds, represent a new technique designed to overcome the limitations of the use of chondrocytes or scaffolds alone.

3. JUSTIFICATION

2. JUSTIFICATION

Nowadays, tissue engineering investigations are widely conducted in the fields of regeneration, restoration, or replacement of defective or injured functional living organs and tissues.[51-53] This represents the main reason for understanding the basic concept of 3D bioprinting as a tool to produce a 3D structure combining living cells and biomaterials, controlling cell proliferation, attachment, differentiation, and migration within 3D structures. Therefore, a significant challenge in otorhinolaryngology and reconstructive plastic surgery is the need for repair or replacement of damaged or absent cartilaginous structures, such as the nose.[54]

According with historical data and previous studies, the current surgical procedures indicated in nasal framework surgery or septal reconstruction have several drawbacks and complications, such as infections, tissue necrosis, and pain. Moreover, a limited number of surgeons worldwide have mastered the skills of using autogenous cartilage.[55] Furthermore, it is well known that the outcome of surgery is often less than perfect.[56-59] Being mandatory to explore novel techniques to improve surgical results and reduced complications as well as drawbacks.

4. OBJETIVES

3. OBJETIVES

Main objective

- Demonstrate the use of 3D-Bioprinting to create a nasal septal cartilage model from rabbit chondrocytes.

Secondary Objective

- Analyzie the in-vitro and in-vivo behavior of the scaffold and cultured cells.
- Analyze the mechanical properties of the scaffold.
- Quantified the chondrogenic potential of the chondrocytes in 3D-bioprinted constructs implanted into rabbit.

5. MATERIAL AND METHODS

MATERIAL AND METHODS

5.1. Scaffold synthesis

Polycaprolactone (PCL) scaffolds were 3D-printed using the FDM technology with a Bioboot 2 bioprinter (Allevi®©, Philadelphia, USA) printer. The PCL polymer was introduced into the bioprinter syringe, melted by heating to 100 °C and subsequently dispensed through a metal needle of 27 G at a pressure of 100 psi and deposition speed of 0.1 mm/seg. Printed scaffolds were sterilized by soaking in 70% ethanol for 1 h and then irradiated under a UV lamp for 30 min (Figure 1, 2, and 3).

5.2. Cell isolation: chondrocyte isolation

Briefly, rabbit ear cartilage was obtained postmortem after removing the hair, skin, and perichondrium of the tissue. Cartilage fragments were sliced into small pieces, transferred into multiwall plates, and washed with washing medium (Hank's balanced salt solution; Gibco; Thermo-Fisher; Sigma-AldrichM San Luis, USA) supplemented with 2% penicillin/streptomycin (P/S) and 2% Fungizone™ (Gibco). Afterwards, the fragments were digested in digestion medium composed of Dulbecco's Modified Eagle Medium (DMEM; Sigma-Aldrich; Thermo-Fisher; Sigma-AldrichM San Luis, USA) containing 1.5 mg/ml collagenase type II (Gibco), 2% P/S, and 2% Fungizone™ overnight at 37 °C with gentle shaking. Subsequently, the digestion medium containing cells was filtered through a 70 μm nylon cell strainer (Corning; New York, USA) to remove tissue residues and clots. Next, cells from the digested tissue were centrifuged at 1500 *rpm* for 5 min and washed three times with washing medium. The cells were then resuspended in culture/expansion medium consisting of low-glucose DMEM supplemented with 10% fetal bovine serum (Gibco) and 1% P/S. Viable cells were determined using the trypan blue dye exclusion assay. Isolated chondrocytes were then cultured until confluence at 37 °C in a humidified CO_2 incubator, and the medium was replaced every 3 days (Figure 3).
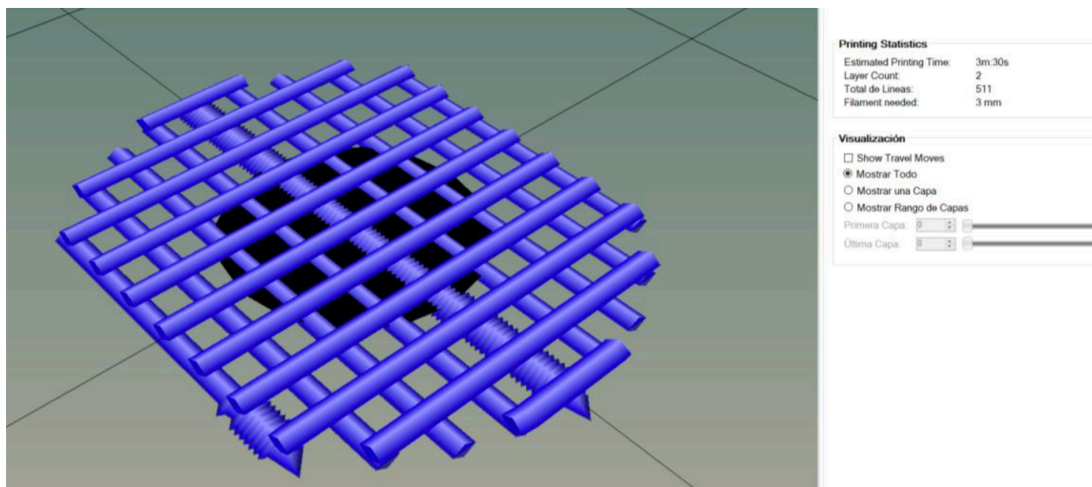
Figure 1. **Two-Layers scafold design**.

Figure 2. **Polycaprolactone scaffolds.**

5.3.   *In vitro* 3D scaffold culture

A total of 50.000 chondrocytes were seeded on top of the scaffolds and allowed to adhere and grow for 1 week in culture medium in a humidified CO_2 incubator, with the medium replaced twice a week. At this specific point, half of the scaffolds were kept

46

in expansion medium under normoxic atmosphere, whereas the other half were cultured under hypoxic conditions (1% O_2) in pro-chondrogenic medium [high glucose DMEM (Sigma-Aldrich) supplemented with 5% fetal bovine serum (Gibco), Insulin-Transferrin-Selenium 1X (Gibco), 100 nM dexamethasone, 100 µg/ml ascorbic acid, 1% P/S, glutamine (Sigma-Aldrich), and TGF-β2 (Peprotech)] for 3 weeks. Samples of cells cultured under both conditions were taken on days 7, 14, and 21. The scaffolds in both conditions were implanted in rabbits on day 21 of culture (Figure 3).
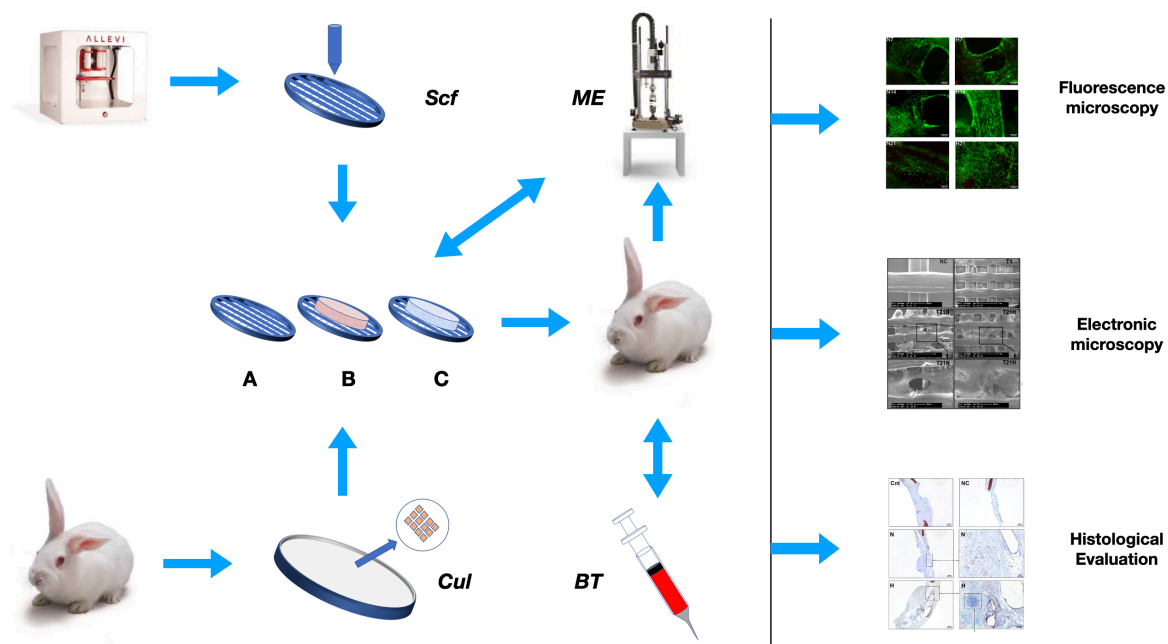
Figure 3. **Study Workflow**. Abreviations: SCF = In vitro scaffold culture; Cul = Cultive; ME = Mechanical Evaluation; BT = Blood Test; A = Scafold without cells; B = Scafold with cells in normoxia; C = Scafold with cells in hypoxia.

5.4. Biochemical evaluation of neo-cartilage

Three samples of each condition and time were digested with 4 U/ml of papain at 60 ºC overnight in phosphate buffered saline (PBS) (Gibco) containing 6 mM L-cysteine hydrochloride and 6 mM ethylenediaminetetraacetic acid disodium salt solution (all from Sigma-Aldrich). Total sulfated GAG were quantified using the Blyscan

Kit (Biocolor; Almeria, Spain) according to the manufacturer's instructions. Next, the absorbance at 656 nm was measured using a HALO LED 96 microplate reader (Dynamica; Livingstone, United Kingdom). Total DNA content was determined using the same digested samples used for the GAG assay following the protocol of the Quant-iT™ dsDNA High-Sensitivity Assay kit (Life Technologies; Carlsbad, USA). DNA yield was measured at an excitation wavelength of 485 nm and an emission wavelength of 528 nm using an Appliskan plate reader (Thermofisher; Waltham, USA) (Figure 3).

The viability of the seeded cells was qualitatively assessed using a live/dead kit (Invitrogen; Waltham, USA). Thus, the scaffolds collected at specific times were washed with PBS (Gibco) for 5 min. Next, an ethidium-calcein staining solution in PBS was added to each well, and the cells were further incubated at 37 °C for 45 min, followed by several washes with PBS. Finally, several images were taken using a Nikon (Tokyo, Japan) 80i fluorescence microscope.

5.5. *In vivo* assay

The Biodonostia Animal Care Committee (San Sebastian, Spain) approved the animal experimentation in accordance with the Spanish Royal Decree 53/2013, European Directive 2010/63/EU, and other relevant guidelines. To simulate the septal cartilage environment, a rabbit ear surgery protocol was proposed because of the low morbidity and high reliability of the structure in mimicking the clinical conditions required to test the scaffold. Twenty adult New Zealand white rabbits weighing 2.0–2.5 kg were included in the study. They were housed with *ad libitum* access to water and food for 3 months under pathogen-free conditions in the barrier facilities of the Biodonostia Health Research Institute (San Sebastian, Spain). They were subjected to daily observation (one animal per cage) to assess their welfare during the study period (8 weeks) (Figure 4).
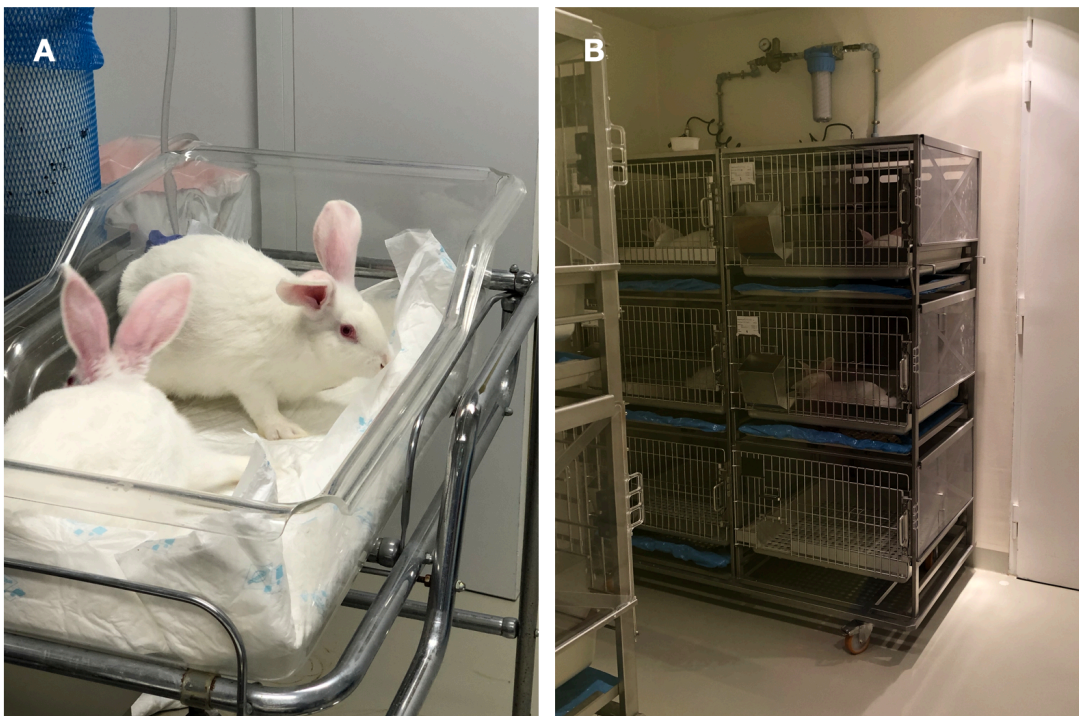
48

Figure 4. **Animal Housing** at Biodonostia Health Research Institute facilities. A) Rabbits before each procedure. B) Animal Housing Room.

Initially, each rabbit underwent surgery in each ear. Briefly, after skin incision, a perichondrium pocket was designed, and a circular biopsy of elastic cartilage of 1 cm diameter was extracted without penetrating the lateral skin. The generation of subperichondrial pockets allows us to simulate the cartilage environment. In the case of the defect group (N= 5 ears), the wound was closed without any kind of insert or scaffold. In the remaining cases, the gap generated in the tissue was refilled with scaffolds without cells (n=5), scaffolds with chondrocytes cultured in non-pro-chondrogenic conditions (n =5), scaffolds with chondrocytes cultured in pro-chondrogenic conditions, and reimplantation of cartilage from the contralateral ear (n=5). To control sepsis throughout the experiment, early markers of sepsis and inflammation were monitored every 14 days (Figure 5 and 6).

Blood samples were collected from the jugular vein of anesthetized rabbits and sent to the Biochemistry Service of our hospital for analysis of protein C-reactive protein and procalcitonin (Figure 7).
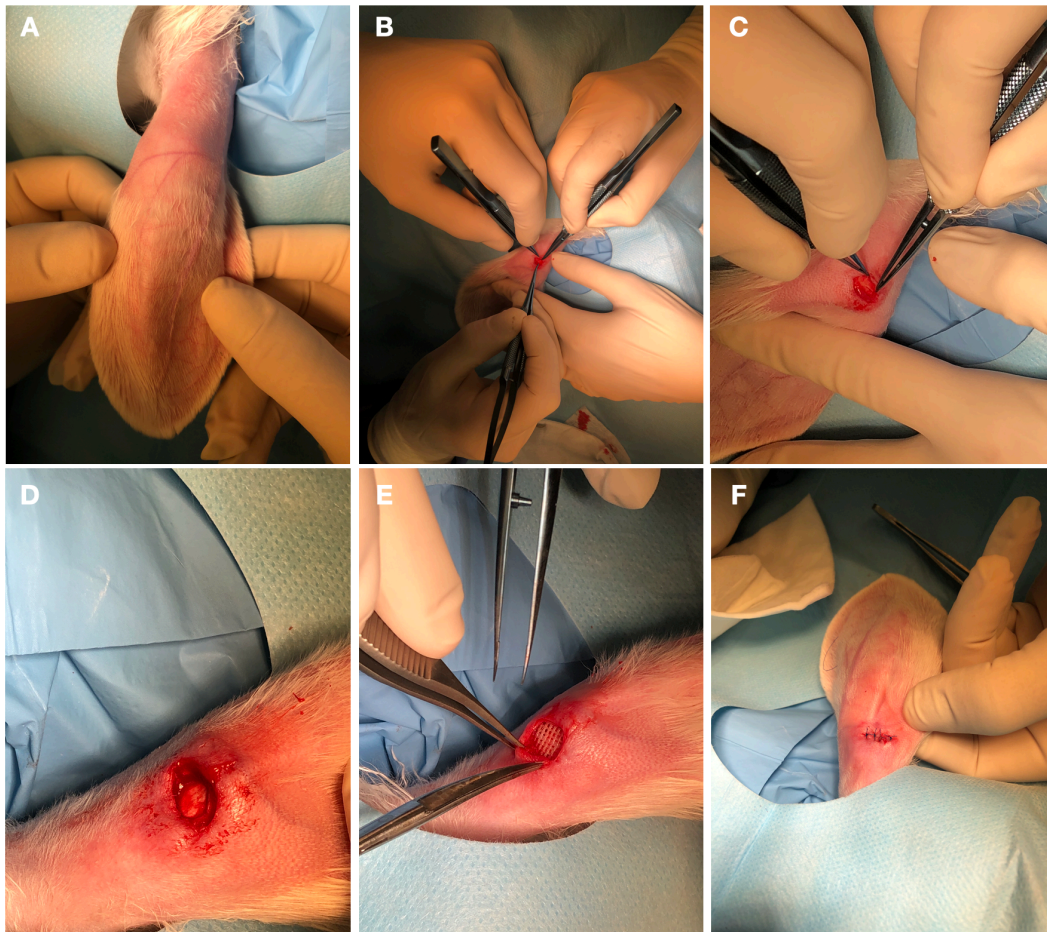
Figure 5. **Surgical Procedure**. A = Surgical bed preparation; B = Skin incision; C= Perichondrial pocket creation; D = Surgical defect; E = Scafold insetting; F = Surgical Closure.
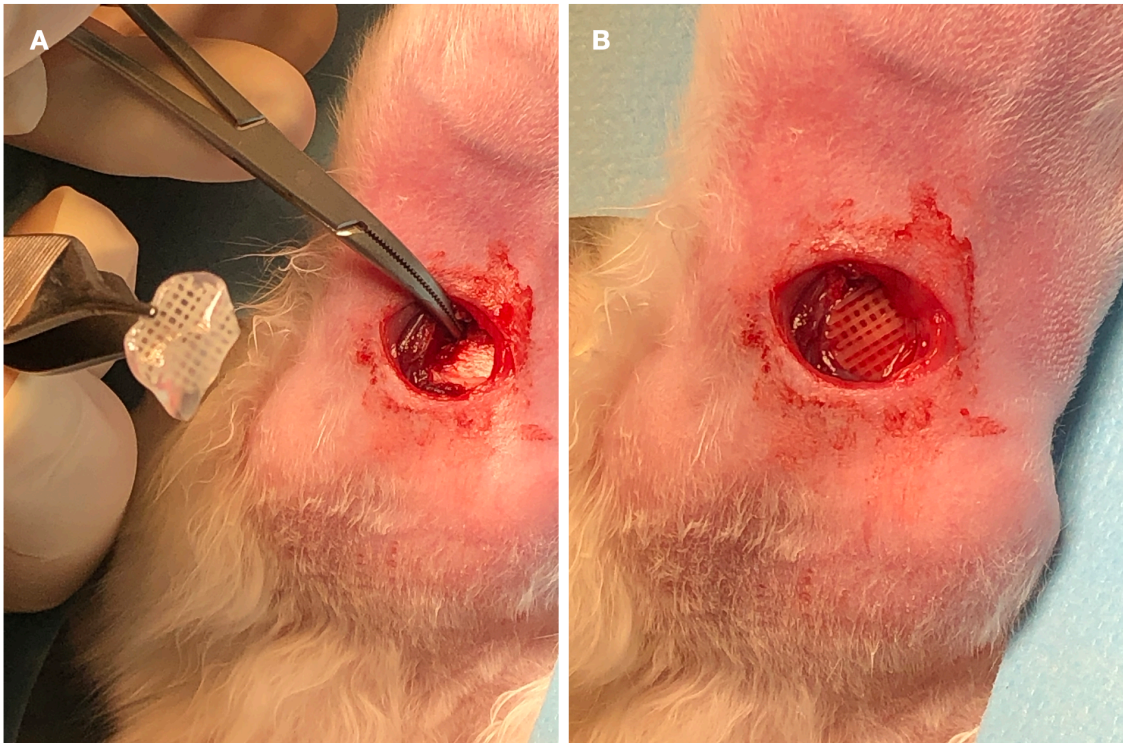
Figure 6. **Surgical Procedure**: A) implantation of a scaffold with chondrocytes cultured in pro-chondrogenic conditions. B) Scafold in place.

Figure 7. **Blood samples collection**.

5.6. Histological assessments: safranine staining and immunofluorescence

Tissue cryosections (7 µm) were sliced with a cryostat and fixed for staining. GAG content was visualized by Safranin O staining, collagen by fast green staining, and cell nuclei by hematoxylin staining. Immunofluorescence was performed using the appropriate primary antibodies for collagen type I (sc-8784; Santa Cruz Biotechnology, USA) and type II (II-II6B3; DSHB, USA) (Figure 3).

5.7. RNA extraction and gene expression analysis

For the *in vitro* experiment, total RNA was isolated from the scaffolds cultured under each condition at specific time points (T7, T14, and T21). For the *in vivo* experiment, tissue samples from the surgical area of each condition with 0.5–1 cm of margins around the inserted scaffold/cartilage/defect were recovered from the ears of the sacrificed rabbits in the third month of stabling. In both experiments, tissues or scaffolds were frozen and lysed with buffer RLT (Qiagen; Hilden, Germany) containing β-mercaptoethanol. All extraction steps were carried out using the RNeasy Mini Kit and RNeasy Plus Micro Kit (Qiagen) for *in vivo* and *in vitro* experiments, respectively. Next, 1 ng of RNA was reverse-transcribed into cDNA using a High-Capacity RNA to DNA kit (Applied Biosystems; Waltham, USA). The cDNA was subsequently pre-amplified using TaqMan® PreAmp Master Mix (Thermofisher; Waltham, USA) according to the manufacturer's instructions. Quantitative real-time PCR was performed using TaqMan® Expression Master Mix and the following TaqMan assay primers: Collagen 2A1 (COL2A1) (Oc03396134_m1), COL1A1 (Oc03396073_g1), Ciclooxigenase 9 (SOX9) (Oc04096872_m1), aggrecan (ACAN) (Oc06726465_m1), and COL10A1 (Oc04097225_s1). The reaction was developed in a CFX384 touch Real-Time PCR Detection System with the following cycling parameters: 50 °C for 2 min, 95 °C for 10 min for polymerase activation, and 40 cycles of 15 s at 95 °C for denaturation and 1 min at 60 °C for annealing. The results were analyzed using the $2^{-\Delta ct}$ method relative to GAPDH (Oc03823402_g1) for *in vitro* samples or the $2^{-\Delta\Delta Ct}$ method for *in vivo* samples (Figure 3).

5.8. Scanning electron microscopy (SEM)

A Philips XL30 CP (Amsterdam, The Netherlands) scanning electron microscope was used to observe the scaffolds and cell morphology with an acceleration voltage of 15 kV at different magnifications. Briefly, the scaffolds were washed three times with Phosphate-Buffered saline (PBS) and fixed with 2.5% glutaraldehyde and 2% paraformaldehyde in PBS for 90 min. Samples were then dehydrated in graded ethanol and air-dried after immersion in hexamethyldisilane (Sigma-Aldrich) for 10 min. Finally, they were coated with a few nanometers of palladium (SC7620 Mini Sputter coater; East Sussex, United Kingdom) (Figure 3).

5.9. Mechanical analysis

To determine the mechanical properties of the cartilage and scaffolds studied, uniaxial compression tests have been carried out using an Instron universal testing machine (Norwood, USA). The Young's modulus was used to calculate the mechanical stress and strain. (Figure 3)

5.10. Statistical analysis

For the statistical analysis, IBM SPSS Statistics 24 (Armonk, New York, USA) was used. After running the Shapiro–Wilk test, in case of the normal distribution of the results, one way ANOVA test was used. For the post hoc analysis, Bonferroni was applied in the case of homoscedasticity; on the contrary, Games-Howell non-parametric test was used. In cases of non-parametric data, for the analysis of the variance, the Kruskal–Wallis test was performed.

5.11. Conflict of interest

6. RESULTS

6. RESULTS

6.1. PCL-scaffold printing and cell seeding

In the field of 3D bioprinting, PCL is a widely used material owing to its biocompatibility.[60] In the present study, the first step of the strategy to improve cartilage regeneration was to develop 3D-printed PCL-based scaffolds. Thus, 2-, 4-, 8-, and 16-layer scaffolds were designed, and their printability was evaluated using an extrusion-based Biobot 3D printer (Allevi) (Figure 8). The optimal parameters for the printing process were set as follows. First, as the fusion point of PCL was near 60 °C, we fixed the extrusion temperature to 100 °C, pursuing the recommendations of Allevi. Next, according to the rheological properties of PCL, the pressure was fixed to 100 psi.
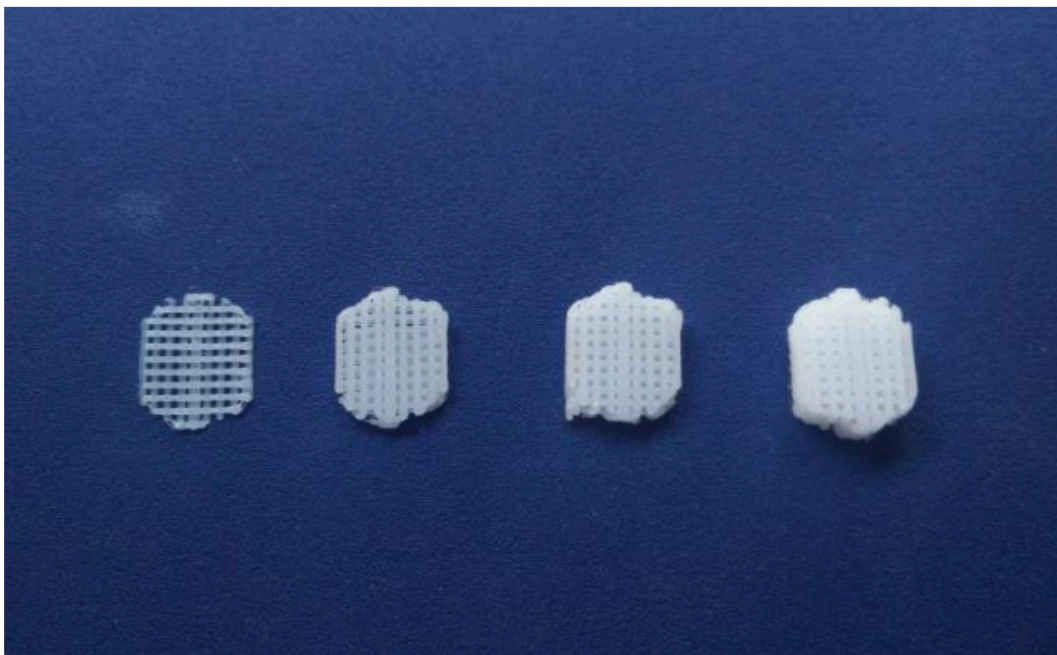

Figure 8. **Scaffolds Fabrication**. A) Schematic figure of whole the strategy B) PCL scaffolds of 2, 4, 8 and 16 layers (from left to right).

The main objective of generating these scaffolds was to regenerate the cartilaginous tissue of the atrium of rabbits. Therefore, considering the thickness of rabbit ear, where the scaffold was going to be implanted, the most suitable type was

the 2-layer scaffold, which had a resolution of 0.1 mm in height and a nozzle diameter of 0.15 mm. The next step was to cellularize scaffolds with chondrocytes. The protocol for extracting the scaffolds from the rabbit ear cartilage was fixed. The designed scaffolds were incubated with chondrocytes in basal medium under normoxic conditions, or under hypoxic conditions in pro-chondrogenic medium. After 21 days of culture, the 3D scaffolds along with the cells were implanted for an *in vivo* test in rabbits for 2 months.

6.2. 3D culture and chondrogenic differentiation *in vitro*

6.2.1. Biochemical characterization of neo-cartilage (GAG/DNA + Live/Dead)

The live/dead assay of chondrogenic cells on the scaffolds was performed in both culture conditions, namely basal medium (normoxia) and pro-chondrogenic medium (hypoxia), for 7, 14, and 21 days to determine the optimum incubation period and conditions to induce cartilage regeneration. Few dead cells were observed on day 7 under normoxic and hypoxic conditions. However, many live cells, which appeared green, were attached to the scaffolds, walls, and holes. In fact, more attached live cells were observed on days 14 and 21 under hypoxic conditions (Figure 9A).

To biochemically characterize the properties of the new extracellular matrix synthesized under normoxia and hypoxia *in vitro*, the content of GAG as a component of the new extracellular matrix was quantified.

GAG synthesis by chondrocytes cultivated under basal conditions (normoxia) and pro-chondrogenic conditions (hypoxia) increased during *in vitro* incubation (Figure 9B). Even though there were no differences in the early (0, 7, and 14 days) days of incubation, GAG difference under both normoxic and hypoxic conditions was significantly higher on day 21 than on day 0. In fact, the maximum GAG values deposited on the scaffold were 38.78 ± 7.99 µg/ml and 29.07 ± 4.00 µg/ml on day 21, respectively. A significant difference between day 0 and 21st, that showed a high activity of chondrogenic differentiation rather than cell proliferation.

GAG values were normalized to DNA content to determine the proportion of GAG synthesized by the cell. Thus, scaffolds with cells after day 7 of incubation showed a higher sGAG/DNA content, reaching the maximum values of 1103.53 ± 177.52 and 1735.45 ± 316.01 on day 21 under normoxia and hypoxia, respectively (Figure 9). This significant difference in sGAG/DNA content between day 0 and 21 indicated a high level of chondrogenic differentiation rather than cell proliferation.

### 6.2.2. Chondrogenic gene expression in the 3D scaffold *in vitro* (qPCR)

The expression of genes associated with chondrogenic differentiation, such as type I and II collagen, aggrecan, and transcription factor Sox9, was detected by qPCR to evaluate the presence of neo-cartilage.

Expression analysis revealed differences in gene expression between the normoxia (N) and hypoxia (H) groups at each time point. In general, the gene expression of collagen 1, 2, aggrecan, and SOX9 in normoxia-cultured scaffolds tended to gradually decrease as the number of days in culture increased. Under hypoxic conditions, only the expression of aggrecan and SOX9 showed the same tendency (Figure 10).

Briefly, the expression of cartilage differentiation markers, such as collagen type I (COL1A) and Sox9, was higher under normoxia on day 7, whereas that of collagen type II (COL2A1) and aggrecan (ACAN) was higher under hypoxic conditions (Figure 10).

Nevertheless, the expression of collagen types I, II, and aggrecan on days 14 and 21 was higher under hypoxic conditions than under normoxic conditions. Moreover, Sox9 expression levels were slightly higher under hypoxic conditions than under normoxic conditions on days 14 and 21 (Figure 3).

(A)
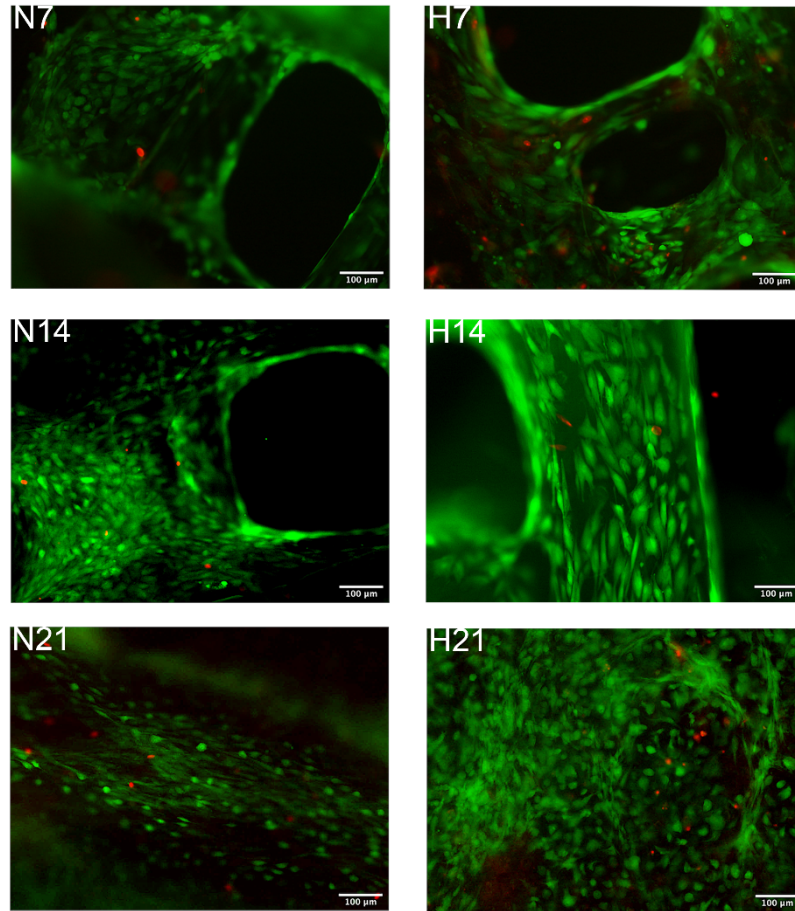
(B)
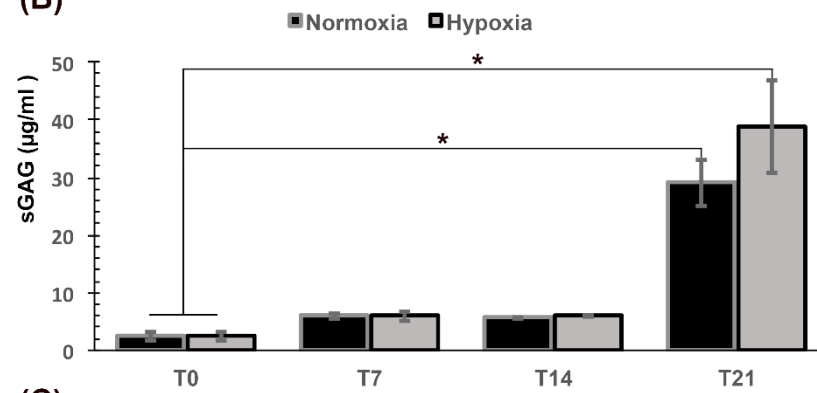
(C)
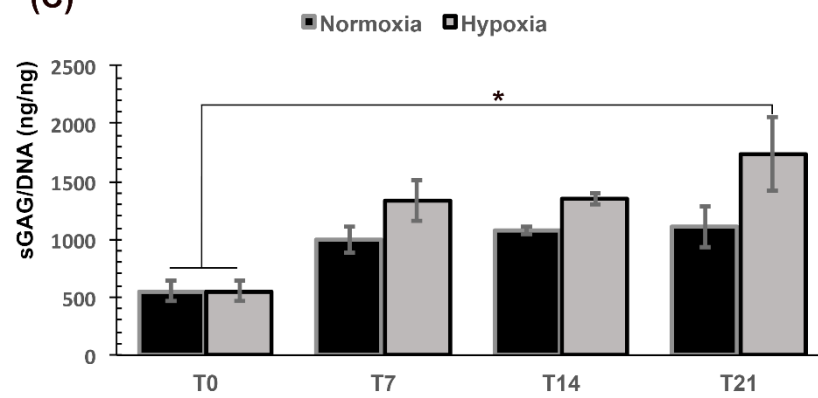
Figure 9. **Biochemical characterization of the neo-cartilage. (A)** Fluorescence microscope images showing chondrocytes growing on scaffolds. Live cells are shown in green (calcein AM) while dead cells are shown in red (ethidium homodimer)**.** N7, N14 and N21 images correspond to chondrocytes growing with basal medium and normoxia on days 7, 14 and 21 respectively. H7, H14, H21 correspond to chondrocytes in culture with pro-chondrogenic medium and hypoxia on days 7, 14 and 21 respectively. Images correspond to an objective of 10X. **(B)** Glicosaminoglycan (sGAG) production by chondrocytes growing on the constructs in normoxic/basal medium versus hypoxic/ pro-chondrogenic conditions in days 0, 7, 14 and 21 of culture. **(C)** Glicosaminoglycan production normalized to DNA content by chondrocytes growing on the scaffolds in normoxic/basal medium versus hypoxic/pro chondrogenic conditions in days 0, 7, 14 and 21 of culture. (* $p<0.05$).

COL1A1

COL2A1

ACAN

SOX9

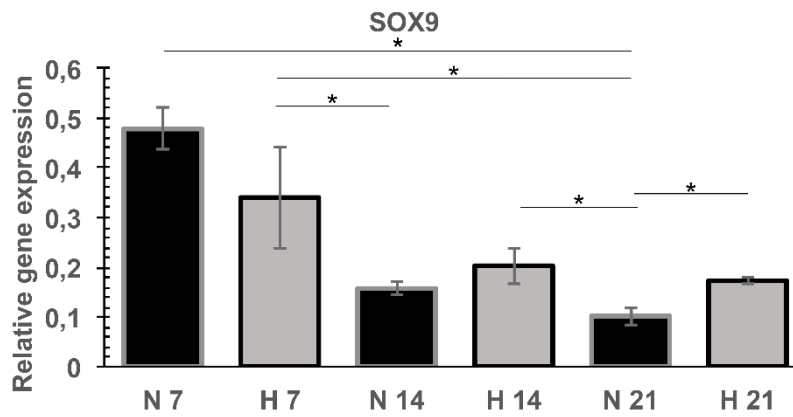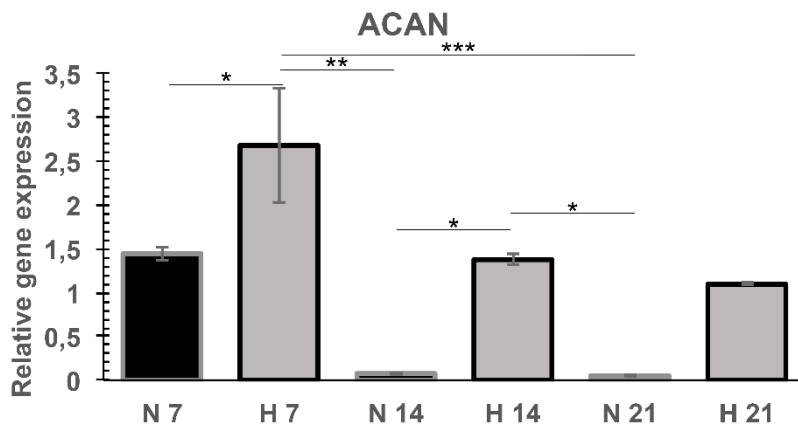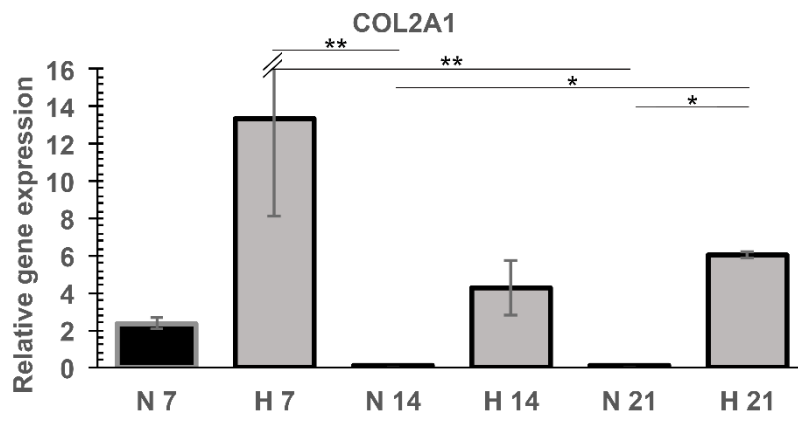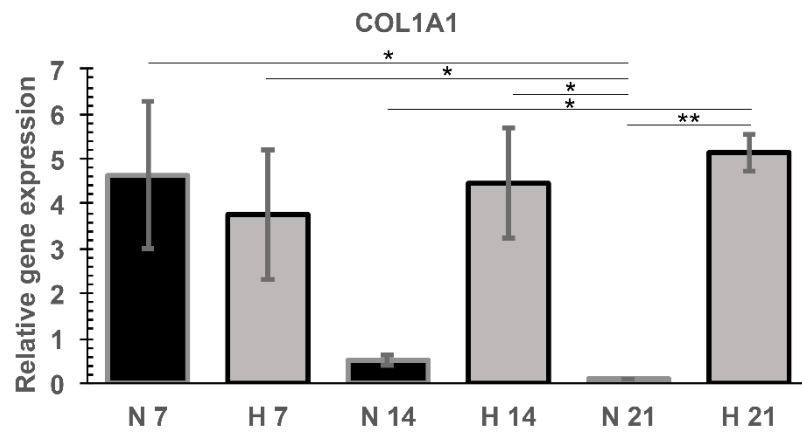Figure 10. **Gene expression profile of in vitro 3D cell culture modelling**. Hyaline cartilage marker expression markers analysis: collagen type I (COL1A1) and type II (COL2A1), aggrecan (ACAN) and chondrogenic differentiation marker (SOX9) in normoxia (N) and hypoxia (H) conditions at day 7, 14 and 21.

6.2.3. Mechanical properties of neo-cartilage

To determine the mechanical properties of the materials studied in this work, uniaxial compression tests were performed. These tests involved compressing cylindrical samples of the studied materials between two parallel plates. During the test, the plates were brought close to each other, and both the force exerted by the plates on the specimen and the separation between them were recorded.

In this experiment, the mechanical properties of four different materials were studied: one corresponding to rabbit cartilage and three others artificially manufactured. All the artificial materials presented the polymeric structure of PCL manufactured by Bioboot 2 bioprinter.

The roughness of the samples and the non-homogeneity in the thickness of the samples made the results of the early phases of the test unreliable. To minimize the effects of settlement of the plates on the specimens, the elastic modulus, or Young's modulus, was determined as the slope of the stress-strain curves between strains of 0.075 and 0.1. For each material studied, the results of at least eight specimens were averaged.

Figure 11A shows an example of the load-strain records obtained for the studied materials. The dispersion of results was high; in these four samples, the softest material corresponded to "Rabbit" and the stiffest to the "NC scaffold group."

To analyze the elastic behavior of the new *in vitro* cartilage, the Young´s modulus was measured. These results suggest that rabbit cartilage is the softest among the materials tested, with an average elastic modulus of 10.8 kPa. Furthermore, the stiffness of all artificial materials was significantly higher than that of the natural material, as shown in Figure 11B. Of note, the elastic modulus of hypoxia specimen

was 110kPa (p<0,001), whereas normoxia and NC group specimen´s values were 21kPa an 39kPa respectively (p<0,05).
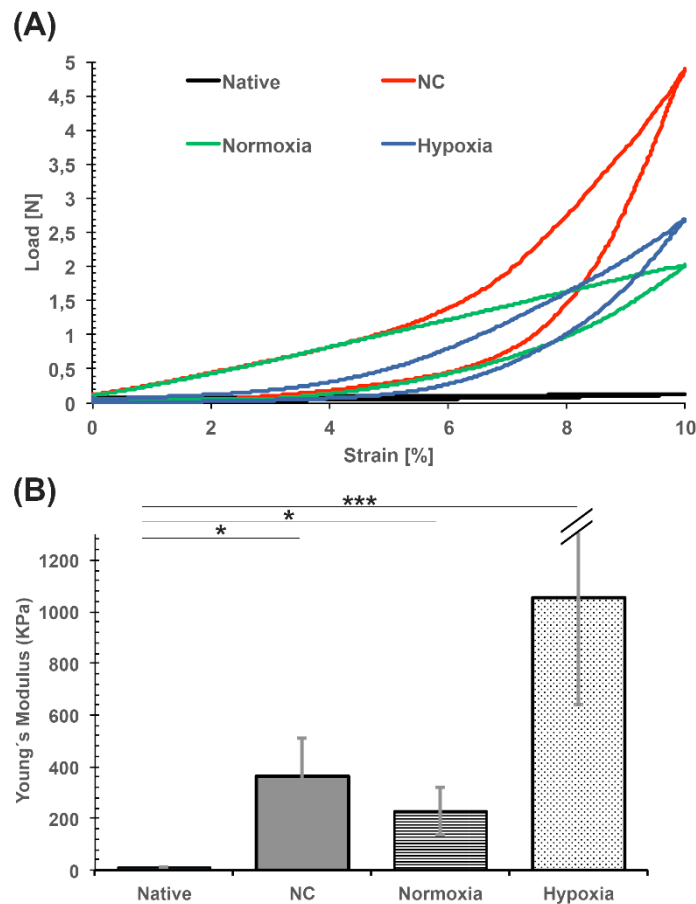
Figure 11**. Biomechanical analysis of the samples**. (A) Example of four load-strain records for the studied material: Native cartilage corresponding to rabbit, No Cells group (NC) corresponding to the scaffold without cells, Normoxia: scaffold with cells cultivated in normoxia and Hypoxia: scaffold with cells cultivated in hypoxia. (* p<0.05, ***p <0.001)

6.2.4. SEM and immunofluorescence analyses of the scaffolds

SEM was performed to observe the microstructure and chondrocyte distribution on the scaffold at different times during cultivation. PCL scaffolds with no cells exhibited

a small widening of the PCL fibers (Figure 12A). This structural modification did not affect the chondrocyte attachment on day 1. On day 21 of culture, under basal normoxic conditions, the chondrocytes had grown as a cell sheet or monolayer around the PCL lattice, whereas under hypoxic conditions, the chondrocytes formed a dense layer that appeared to be extracellular matrix deposition. Immunofluorescence staining of the scaffolds was performed for collagen 1 and 2 proteins as markers of cartilage-like tissue extracellular matrix deposition (figure 12B). The presence of both collagens (1 and 2) was observed, forming a thick layer of extracellular matrix that folded over itself under hypoxic conditions (Figure 12B - T21H). As presented in the image, collagens 1 and 2 are distributed in two different layers under hypoxic conditions, whereas under normoxic conditions, there seems to be a mixed pattern of distribution along the cell sheet.

(A)
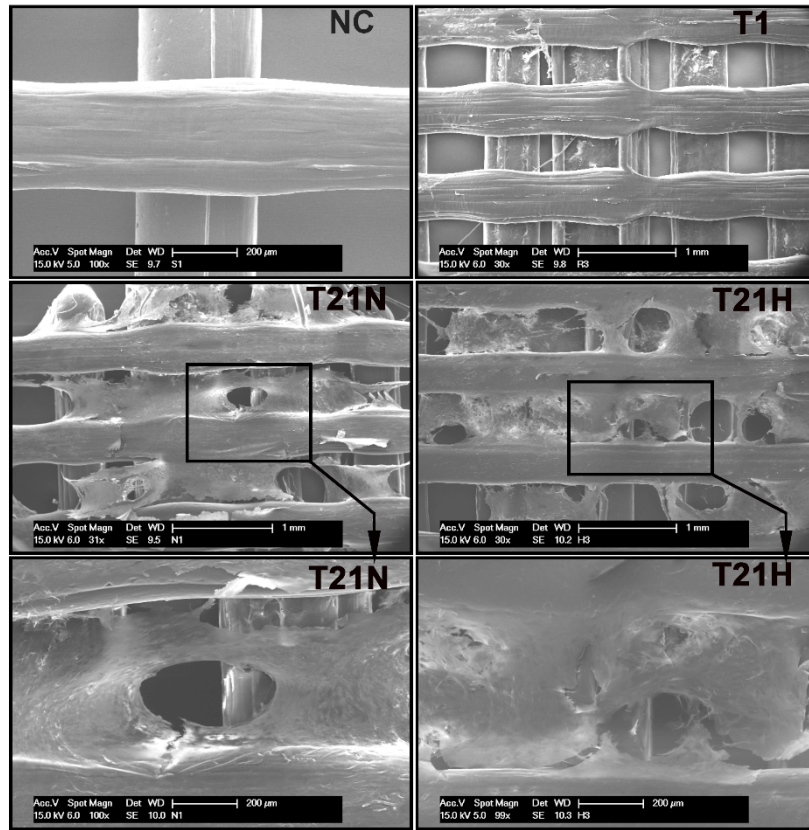
(B)
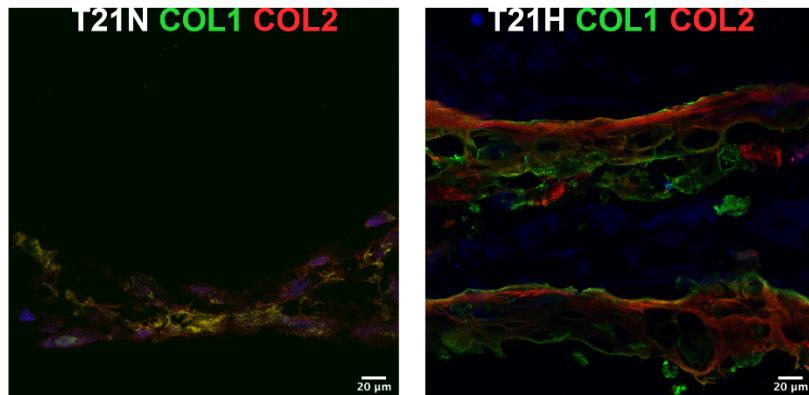
Figure 12. (A) **Scanning electron microscopy images of scaffolds**. NC: Scaffolds without cells; T1: Adhesion of chondrocytes in culture on top of the scaffolds in first 24 hours of culture; T21N: chondrocytes in proliferation medium (normoxic) day 21 and

H21N: chondrocytes in prochondrogenic medium (hypoxia) day 21. (B) **Immunofluorescence of collagen 1 and 2** (COL1, COL2 respectively) for chondrocytes in proliferation medium (T21N) and chondrogenic medium(T21H) on day 21 of culture.

6.3. *In vivo* assay

The New Zealand white rabbit model is an *in vivo* model used for the preliminary observation of tissue-engineered cartilage tissue. *In vitro* co-culture of rabbit chondrocytes under basal and pro-chondrogenic conditions into 3D-printed PCL scaffolds with an internal spherical porous architecture resulted in the growth of cartilage-like tissue after 21 days.
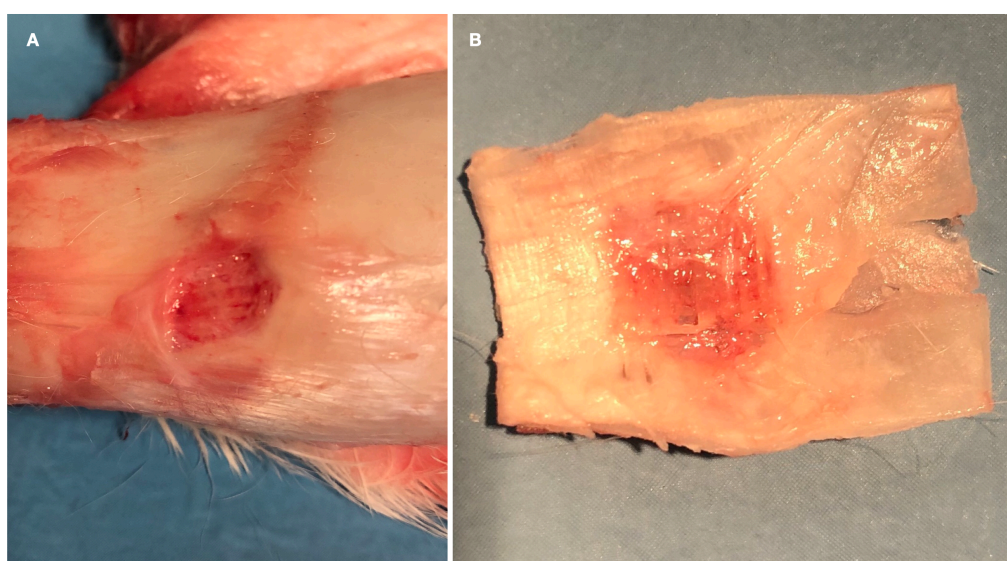
Figure 13. **Surgical Specimen**. Tissue analysis of a scaffold with chondrocytes cultured in pro-chondrogenic conditions after the experimental period properly integrated.

Twenty specimens from the *in vivo* study were analyzed. The PCL cellular and acellular scaffolds located in the sub-perichondral pocket were well-tolerated by the animals, with no major complications (Figure 13). However, hypertrophic scar formation was observed in one rabbit from the acellular scaffold group (Figure 14).

Reactive C protein and procalcitonin levels in blood showed no variation during the experimental period.

Figure 14. **Complications.** A case of hypertrophic scar formation in one rabbit from the acellular scaffold group.

6.3.1. Chondrogenic gene expression in the 3D scaffold after *in vivo* (qPCR) implantation

The presence of neo-cartilage was evaluated by measuring the expression of chondrogenic gene markers after 2 months of *in vivo* experiments on rabbits. Three experimental groups were compared: scaffold without cells (NC), scaffold with cells grown under basal normoxic conditions, and scaffold with cells grown under pro-chondrogenic hypoxic conditions.

Quantitative PCR results revealed that the expression of collagen type I, type II, aggrecan (ACAN), and Sox9 tended to be higher under hypoxic conditions than under normoxia. Thus, collagen type I and Sox9 expression was slightly higher in the hypoxia group than in the acellular scaffold group (NC) (Figure 15A).

In addition, the expression of type X collagen (COLX), a marker for new bone formation in cartilages, was higher in the NC group (Figure 15A).

6.3.2. Histological evaluation and immunofluorescence analysis of the neo-cartilage formation *in vivo*

After 3 months, histological evaluation of the *in vivo* models was performed. Safranine O staining revealed a significant accumulation of GAGs in rabbits implanted with the scaffold containing cells cultivated under hypoxic conditions (Figure 15B). There was no evidence of neo-cartilage formation in any of the experimental groups (Figure 15B).

Along with this, cartilage regeneration was observed close to the scaffold, as shown in Figure 15 (B–H), close to the typical histological cartilage image presented in Figure 15 (B–NA).

The growth of histologically normal-appearing cartilage was noted in the hypoxia group after 8 weeks of *in vivo* culture and was confirmed by immunohistochemical staining of type I and II collagen. Hyaline cartilage architecture was determined by histological analysis as having dense collagen deposition, with lacunae surrounding differentiated chondrocytes.

(A)

(B)
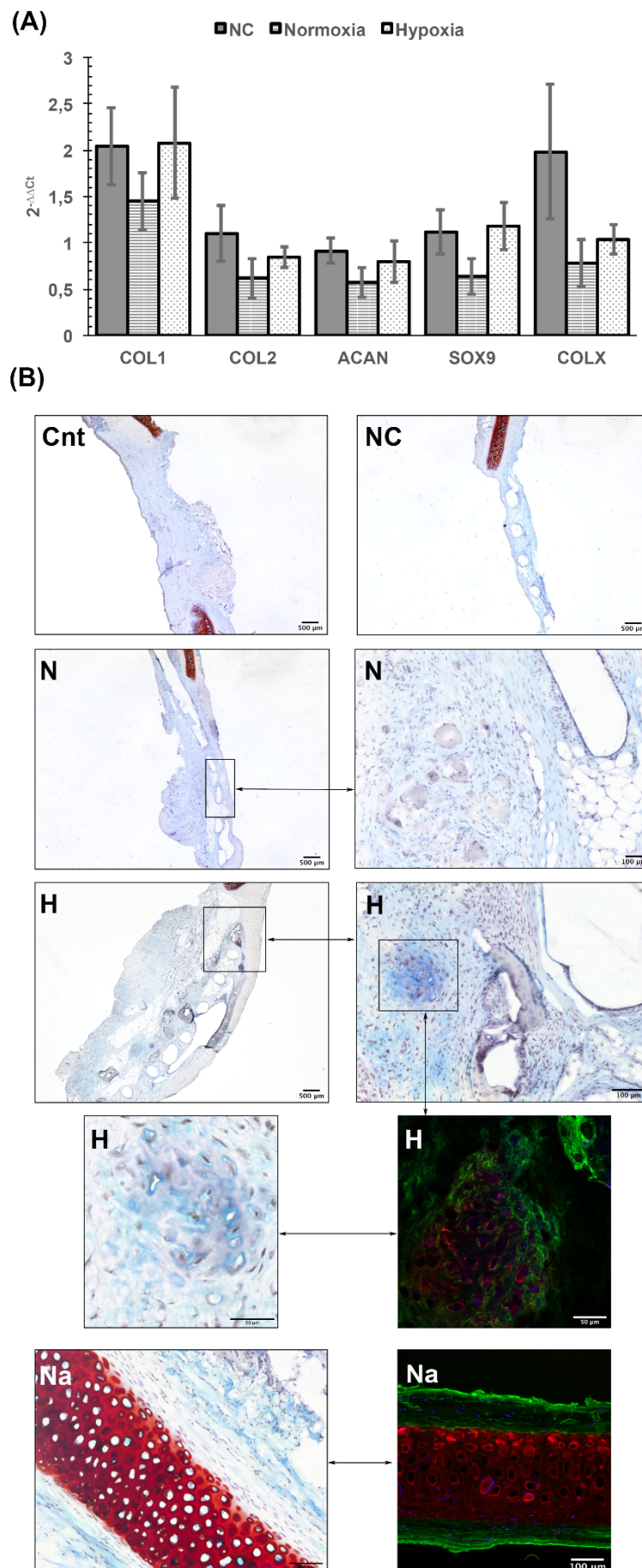
Figure 15. **(A) Chondrogenic gene expression after 2 months of** *in vivo* **experiment on rabbit ears.** Histogram indicates fold expression of each study group relative to control without scaffold COL1 and COL2: collagen 1 and 2 respectively; ACAN: aggrecan; SOX9: transcription factor SOX9; COLX: collagen 10. **(B) Histological evaluation of the cartilage after 3 months** *in vivo* **experiment.** Examples of Safranine O and immunofluorescence staining of each group of treatment, controls and native tissue are represented. Cnt: control; NC: scaffold without cells; N: normoxia, H: hypoxia, Na: native tissue.

7. DISCUSSION

7. DISCUSSION

In the present study, the viability and effectiveness of 3D-bioprinting in generating a biocompatible PCL cartilage scaffold were evaluated. Rabbit primary chondrocytes were cultured *in vitro* under pre- and pro-chondrogenic conditions for 21 days. Additionally, the expression of GAG, DNA, collagen I, II, and X in the experimental specimens was measured. Next, in the evaluation of cartilage formation *in vivo*, 3D scaffolds containing cells grown under pre- and pro-chondrogenic conditions were implanted into the auricular subperichondrial pocket of rabbit ear to simulate the nasal septal cartilage condition for 8 weeks. Histological analysis of these scaffolds, with Safranin and immunohistochemical staining, revealed the presence of collagen I and II as well as cartilage regeneration.

Here, we have described the limitations, complications, and drawbacks of the current surgical procedures indicated in nasal framework surgery or septal reconstruction, as well as the fact that only a limited number of surgeons worldwide have mastered the skills of utilizing autogenous cartilage.[55] In this vein, various options to avoid the use of autologous rib reconstruction have been described, such as the use of prefabricated, synthetic MedPor (Stryker Corporation, Kalamazoo, Michigan, USA) or porous, high-density polyethylene implants.[10] However, personalized frameworks are not available for each patient-specific anatomical defect. Furthermore, despite being FDA-approved, MedPor still has a high incidence of framework extrusion and soft tissue necrosis, compared to autologous cartilage reconstruction.[11]

In recent years, the use of biomedical scaffolds made of natural or synthetic polymers has emerged as a potential tool for nasal cartilage repair.[12,13] The use of this scaffold technology allows manufacturing improvement via an individually calibrated process, making it possible to modify the porosity (pore size distribution, pore volume, and pore interconnectivity) of scaffolds to increase cell affinity, proliferation, migration, attachment, and differentiation, and even enabling nutrient and oxygen transport in a purpose-built manner.[15,16]

In our current study, the FDM 3D-printing method was employed for generating the scaffolds.[61,62] This technique is one of the most reliable methods for fabricating 3D-printed scaffolds because of its low cost, ease of use, availability of a great variety of biomaterials, and good mechanical properties. However, the obvious disadvantages of this technique include material restrictions related to thermoplastic polymers and low effectiveness due to high manufacturing temperature.

PCL is the most commonly used biopolymer.[63] It is a biocompatible and biodegradable synthetic polymer with adequate mechanical strength and durability for cartilage regeneration. The advantageous rheological and viscoelastic properties of this polymer render it easy to manufacture and manipulate into different implants and devices.[62] In addition, its excellent mechanical properties (it resists deformity from scar contraction during the healing process) and slow biodegradation support its use in nasal reconstruction.[61] However, it is important to note that the mechanical properties of bioengineered cartilage are modulated by the deposition of GAGs and collagens and by the cell type used.[64]

Ferril *et al.* have reported the characteristics that define an ideal alloplastic material. They highlighted that implants need to be noncarcinogenic, nonallergenic, readily available, resistant to mechanical strain, and entirely absorbable, whilst still providing the desired outcome.[65] PCL implants are produced with a compressive stiffness range between 2.74 and 55.95 MPa, according to the processing parameters, and this range is inclusive of native cartilage parameters (12.8–22.5 MPa).[67,68] Thus, the mechanical properties of PCL implants can match those of cartilage without difficulty. In the present study, when Young's modulus was applied to our scaffold, both mechanical stress and strain exhibited higher resistance than the cartilage. Although adverse events or complications such as extrusion or skin erosion were not observed, this can be related to the short follow-up period, considering that one case of keloid formation was observed. More recently, Nam *et al.* evaluated different disc-shaped scaffolds with 100-, 200-, 300-, and 400-μm pores fabricated using PCL, wherea chondrocytes and fibroblasts were seeded and cultured with mild shaking until 56 days. After a careful morphological and quantitative analysis, the authors confirmed that

chondrocytes and fibroblasts proliferated most extensively at the 400-μm pore size scaffold.[69] To examine this in more detail, we are currently conducting a translational study to evaluate the behavior of the bio-scaffold in 6- and 12-month periods.

As previously described, type II collagen is primarily found in hyaline cartilages, such as articular and nasoseptal cartilage, and is considered a first-choice cartilage substitute in many surgical procedures.[70] Unfortunately, type II collagen shows unwanted arthritogenic activities.[71,72] In contrast, type I collagen does not elicit adverse immune reactions, particularly in the absence of its telopeptides, and lacks arthritogenic effects.[73,74] Additionally, owing to its higher rate of biocompatibility, type I collagen is commonly used in cartilage tissue engineering.[75] In this regard, our study revealed the high proliferation of both type I and II collagen, with the type I collagen being the most commonly observed collagen.

Regarding histological cell proliferation, the most important finding in our study was the clear proliferative cartilage formation. After 21 days, the *in vivo* model exhibited a high percentage of cross-sectional area occupied by GAG-positive cells, and type 2 collagen formation was observed through immunostaining, with cluster formation of GAG-positive cells representing a definitive sign of proliferation. The results can be considered a qualitative evidence of cartilage proliferation over the bioprinted scaffold. We tried to quantitatively estimate the proliferation rates, but we could not do it using an automatized method because of the problems related to segmentation of the histological images and the consequent underestimation of cell growth. Moreover, the manual counting procedure was not described owing to the absence of a general pattern.

Currently, the main obstacles in this kind of procedure include the need for designing a nasal framework with a similar anatomical size and shape. Several authors have described previous experience using bioresorbable polymer into a negative clay mold of the cartilage structure.[76-78] In this regard, the application of computer-aided design and computer-aided manufacturing techniques may overcome this limitation.

It is also necessary to mention the unfavorable properties of synthetic materials for use in cartilage regeneration, such as their low biocompatibility, low bioactivity, and potential aseptic inflammation caused by their degradation products when implanted into immunocompetent large animal models and humans. Some authors have argued against the use of synthetic polymers for cartilage regeneration. Conversely, the authors claimed that the use of natural polymers improves biocompatibility and biological activity whilst reducing the immunogenicity and cytotoxicity of their degradation products, making them a favorable biomimetic scaffold for cartilage regeneration.[79,80] Hence, natural ECM-derived scaffolds have become popular in recent years owing to their natural composition and natively structured microenvironment.[81] Wiggenhauser *et al.*[82] recommend the use of porcine septal cartilage to develop a matrix derivative that is highly suitable for cartilage scaffolding with human chondrocytes as a decellularized extracellular cartilage matrix. Furthermore, these authors had previously shown the efficacy and safety of these types of scaffolds.[83-86] As highlighted by Moller *et al.*[81] hydrogel-based scaffolds also constitute a valid alternative. Their high-water content gives them a structural similarity to the cartilage ECM, conceptually improving the regeneration environment.[87,88] In the case of hydrogels, one of the shortcomings is their viscoelastic properties, which hamper their good printing fidelity. Another problem is their mechanical properties, such as strength and stiffness, which make them difficult to handle during transplantation. Moller *et al.* revealed the viability of co-culture of human nasal chondrocytes and human bone marrow-derived MSCs, rather than a single cell type alone, using a specific combination at a 20/80 ratio, which is an optimal ratio for the induction of cartilage regeneration.[89-94]

Although we were able to show the effectiveness of this technique, owing to the ear rabbit size, the use of 2-layer PCL-scaffold depends on the type of defect, and a multilayer cellular PCL-scaffold can be used. Moreover, the main goal of this study was to evaluate the possibility of emulating a hyaline cartilage structure, and our results suggest that other cartilage structures (*e.g.,* ear cartilage, articular cartilage, or tracheal cartilage) can be substituted using the same approach.

Our group is currently conducting a study to characterize and test our method using human nasal septal cartilage to create a human-based 3D-bioprinted nasal septal cartilage to establish the basis for a preclinical study.

Discussion

Discussion

8. CONCLUSION

8. CONCLUSION

With the development of new technologies, the range of options to try to treat hyaline cartilage defectsf widens and 3D printing emerges as an option that allows obtaining personalized grafts (scaffold) and treating each patient individually. In this study we demonstrated the viability and feasibility of a 3D-Bioprinting co-cultured method to generate a tissue-engineered nasal septal cartilage.

9. REFERENCES

9. REFERENCES

1. Hull CW, inventor; Uvp Inc., original assignee. Apparatus for production of three-dimensional objects by stereolithography (1986). United States Patent US4575330A. Available at: https://www.google.com/patents/US4575330. Last accessed: 11 october 2020

2. Kruth JP, Leu MC, Nakagawa T. Progress in Additive Manufacturing and Rapid Prototyping. CIRP Ann-Manuf Techn. 1998;47(2): 525-40.

3. Melchels FPW, Domingos MAN, Klein T, Malda J, Bartolo P, Hutmacher D. Additive manufacturing of tissues and organs. Prog Polym Sci. 2012;37:1079-104.

4. Bak D. Rapid prototyping or rapid production? 3D printing processes move industry towards the latter. Assembly Autom. 2003;23:340-5.

5. Setton LA, Elliott DM, Mow VC. Altered mechanics of cartilage with osteoarthritis: human osteoarthritis and an experimental model of joint degeneration. Osteoarthritis Cartilage 1999;7:2.

6. Jackson DW, Scheer MJ, Simon TM. Cartilage substitutes: overview of basic science and treatment options. J. Am. Acad. Orthop Surg 2001;9:37.

7. Rengier F, Mehndiratta A, von Tengg-Kobligk H, Zechmann CM, Unterhinninghofen R, Kauczor HU, et al. 3D printing based on imaging data: review of medical applications. Int J Comput Assist Radiol Surg. 2010;5:335-41.

8. Kushnaryov A, Yamaguchi T, Briggs KK, Wong VW, Reuther M, Neuman M, et al. Evaluation of autogenous engineered septal cartilage grafts in rabbits: a minimally invasive preclinical model. Otolaryngol Neck Surg. 2013;149(2 suppl):37-38.

9. Fulco I, Miot S, Haug MD, Barbero A, Wixmerten A, Feliciano S, et al. Engineered autologous cartilage tissue for nasal reconstruction after tumour resection: an observational first-in-human trial. Lancet. 2014;384:337-46.

10. Romo T 3rd, Presti PM, Yalamanchili HR. Medpor alternative for microtia repair. Facial Plast Surg Clin North Am. 2006;14:129-136.

11. Zhao YY, Zhuang HX, Jiang HY, Jiang WJ, Hu XG, Hu SD, et al. Clinical application of three methods for total ear reconstruction. Zhonghua Zheng Xing Wai Ke Za Zhi. 2008;24:287-90.

12. Tian H, Tang Z, Zhuang X, Chen X, Jing X. Biodegradable synthetic polymers: preparation, functionalization and biomedical application. Prog Polym Sci. 2012;37(2):237-80.

13. O'Brien FJ. Biomaterials and scaffolds for tissue engineering. Mater Today. 2011; 14:88-95.

14. Bose S, Vahabzadeh S, Bandyopadhyay A. Bone tissue engineering using 3D printing. Mater Today. 2013;16:496-504.

15. Gauvin R, Chen YC, Lee JW, Soman P, Zorlutuna P, Nichol JW, et al. Microfabrication of complex porous tissue engineering scaffolds using 3D projection stereolithography. Biomaterials. 2012; 33:3824-34.

16. Martin JR, Gupta MK, Page JM, Yu F, Davidson JM, Guelcher SA, et al. A porous tissue engineering scaffold selectively degraded by cell-generated reactive oxygen species. Biomaterials. 2014;35:3766-76.

17. Teh TK, Toh SL, Goh JC. Aligned hybrid silk scaffold for enhanced differentiation of mesenchymal stem cells into ligament fibroblasts. Tissue Eng Part C Methods. 2011 Jun;17(6):687-703.

18. Unadkat HV, Hulsman M, Cornelissen K, Papenburg BJ, Truckenmüller RK, Carpenter AE, et al. An algorithm-based topographical biomaterials library to instruct cell fate. Proc Natl Acad Sci USA. 2011 Oct 4;108:16565-70.

19. Thomas V, Jose MV, Chowdhury S, Sullivan JF, Dean DR, Vohra YK. Mechano-morphological studies of aligned nanofibrous scaffolds of polycaprolactone fabricated by electrospinning. J Biomater Sci Polym Ed. 2006;17:969-84.

20. Chiesa-Estomba C. González Fernández, I. Iglesias Otero A.. 3D Printing for Biomedical Applications: Where Are We Now? Eur. Med. J. 2017, 2, 16–22.

21. Du Y et al. Microsphere-based selective laser sintering for building macroporous bone scaffolds with controlled microstructure and excellent biocompatibility. Colloids Surf B:Biointerfaces. 2015;135:81-9.

22. Chen CH et al. Surface modification of polycaprolactone scaffolds fabricated via selective laser sintering for cartilage tissue engineering. Mater Sci Eng C. 2014;40:389-97.

23. Ciocca L et al. Direct metal laser sintering (DMLS) of a customized titanium mesh for prosthetically guided bone regeneration of atrophic maxillary arches. Med Biol Eng Comput. 2011;49:1347-52.

24. Shafiee A, Seyedjafari E, Sadat Taherzadeh E, Dinarvand P, Soleimani M, Ai J. Enhanced chondrogenesis of human nasal septum derived progenitors on nanofibrous scaffolds. Mater Sci Eng C Mater Biol Appl. 2014;40:445-54.

25. Bedi A, Feeley BT, Williams RJ 3rd. Management of articular cartilage defects of the knee. J Bone Joint Surg Am. 2010;92:994-1009.

26. Discher DE, Janmey P, Wang YL. Tissue cells feel and respond to the stiffness of their substrate. Science. 2005;310:1139-43.

27. Homicz MR, McGowan KB, Lottman LM, Beh G, Sah RL, Watson D. A compositional analysis of human nasal septal cartilage. Arch Facial Plast Surg. 2003;5:53-8.

28. Bas O, De-Juan-Pardo EM, Meinert C, D'Angella D, Baldwin JG, Bray LJ, et al. Biofabricated soft network composites for cartilage tissue engineering. Biofabrication. 2017;9:025014.

29. Kafienah W, Jakob M, Démarteau O, Frazer A, Barker MD, Martin I, et al. Three-dimensional tissue engineering of hyaline cartilage: Comparison of adult nasal and articular chondrocytes. Tissue Eng. 2002;8:817–826.

30. Rotter N, Bonassar LJ, Tobias G, Lebl M, Roy AK, Vacanti CA. Age dependence of biochemical and biomechanical properties of tissue-engineered human septal cartilage. Biomaterials. 2002;23:3087–94.

31. Tay AG, Farhadi J, Suetterlin R, Pierer G, Heberer M, Martin I. Cell yield, proliferation, and postexpansion differentiation capacity of human ear, nasal, and rib chondrocytes. Tissue Eng. 2004;10:762–770.

32. Liu X, Sun H, Yan D, Zhang L, Lv X, Liu T, et al. In vivo ectopic chondrogenesis of BMSCs directed by mature chondrocytes. Biomaterials 2010;31:9406–9414.

33. Keller B, Yang T, Chen Y, Munivez E, Bertin T, Zabel B, et al. Interaction of TGFbeta and BMP signaling pathways during chondrogenesis. PLoS One 2011;6:316421.

34. Kim JS, Ryoo ZY, Chun JS. Cytokine-like (Cytl1) regulates the chondrogenesis of mesenchymal cells. J Biol Chem 2007;282:29359–29367.

35. Choi YS, Lim SM, Shin HC, Lee CW, Kim SL, Kim DI. Chondrogenesis of human periostiumderived progenitor cells in atelocollagen. Biotechnol Lett 2007;29:323–329.

36. Mo XT, Guo SC, Xie HQ, Deng L, Zhi W, Xiang Z, et al. Variations in the ratios of co-cultured mesenchymal stem cells and chondrocytes regulate the expression of cartilaginous and osseous phenotype in alginate constructs. Bone 2009;45:42–51.

37. Shieh SJ, Terada S, Vacanti JP. Tissue engineering auricular reconstruction: In vitro and in vivo studies. Biomaterials 2004;25:1545–1557.

38. Zhou L, Pomerantseva I, Bassett EK, Bowley CM, Zhao X, Bichara DA, et al. Engineering ear constructs with a composite scaffold to maintain dimensions. Tissue Eng Part A 2011;17:1573–1581.

39. Xue J, Feng B, Zheng R, Lu Y, Zhou G, Liu W, et al. Engineering earshaped cartilage using electrospun fibrous membranes of gelatin/polycaprolactone. Biomaterials 2013;34:2624–2631.

40. Ruszymah BH, Chua KH, Mazlyzam AL, Aminuddin BS. Formation of tissue engineered composite construct of cartilage and skin using high density polyethylene as inner scaffold in the shape of human helix. Int J Pediatr Otorhinolaryngol 2011;75:805–810.

41. Yanaga H, Imai K, Fujimoto T, Yanaga K. Generating ears from cultured autologous auricular chondrocytes by using two-stage implantation in treatment of microtia. Plast Reconstr Surg 2009;124:817–825.

42. Von Der Mark K, Gauss V, Von Der Mark H, Mueller P. Relationship between cell shape and type of collagen synthesised as chondrocytes lose their cartilage phenotype in culture. Nature 1977;267:531–532.

43. Kusuhara H, Isogai N, Enjo M, Otani H, Ikada Y, Jacquet R, et al. Tissue engineering a model for the human ear: assessment of size, shape, morphology, and gene expression following seeding of different chondrocytes. Wound Repair Regen 2009;17:136–146.

44. Tsutsumi S, Shimazu A, Miyazaki K, Pan H, Koike C, Yoshida E, et al. Retention of multilineage differentiation potential of mesenchymal cells during proliferation in response to FGF. Biochem Biophys Res Commun 2011;288:413–419.

45. Martin I, Shastri VP, Padera RF, Yang J, Mackay AJ, Langer R, et al. Selective differentiation of mammalian bone marrow stromal cells cultured on three-dimensional polymer foams. J Biomed Mater Res 2001;55:229–235.

46. Hwang NS, Elisseeff J. Application of stem cells for articular cartilage regeneration. J Knee Surg 2009;22:60

47. Hickok NJ, Haas AR, Tuan RS. Regulation of chondrocyte differentiation and maturation. Microsc Res Tech 1998;43:174–190.

48. Merceron C, Vinatier C, Portron S, Masson M, Amiaud J, Guigand L, et al. Differential effects of hypoxia on osteochondrogenic potential of human adipose-derived stem cells. Am J Physiol Cell Physiol 2010;298:C355–C364.

49. Apelgren P, Amoroso M, Lindahl A, Brantsing C, Rotter N, Gatenholm P, Kölby L. Chondrocytes and stem cells in 3D-bioprinted structures create human cartilage in vivo. PLoS One. 2017;12:e0189428.

50. Niermeyer WL, Rodman C, Li MM, Chiang T. Tissue engineering applications in otolaryngology-The state of translation. Laryngoscope Investig Otolaryngol. 2020;5:630-48.

51. Dhandayuthapani B, Yoshida Y, Maekawa T, Kumar S. Polymeric scaffolds in tissue engineering application: a review. Int J Polym Sci. 2011;2011:290602.

52. Atala A. Tissue engineering of reproductive tissues and organs. Fertil Steril. 2012;98:21-9.

53. Forbes SJ, Rosenthal N. Preparing the ground for tissue regeneration: from mechanism to therapy. Nat Med. 2014;20:857-69.

54. Lindahl A. From gristle to chondrocyte transplantation: treatment of cartilage injuries. Philos Trans R Soc Lond B Biol Sci. 2015; 370(1680):20140369.

55. Brent B. The correction of microtia with autogenous cartilage grafts, the classic deformity. Plast Reconstr Surg. 1980;66:1-12.

56. Firmin F. State-of-the-art autogenous ear reconstruction in cases of microtia. Adv Otorhinolaryngol.2010; 68:25±52.

57. Zopf DA, Iams W, Kim JC, Baker SR, Moyer JS. Full-thickness skin graft overlying a separately harvested auricular cartilage graft for nasal alar reconstruction. JAMA Facial Plast Surg. 2013; 15:131-4.

58. Firmin F, Marchac A. A novel algorithm for autologous ear reconstruction. Semin Plast Surg. 2011; 25:257-64.

59. Osorno G. Autogenous rib cartilage reconstruction of congenital ear defects: report of 110 cases with Brent's technique. Plast Reconstr Surg. 1999;104:1951-62.

60. Kim DH, Yun WS, Shim JH, Park KH, Choi D, Park MI, Hwang SH, Kim SW. Clinical Application of 3-Dimensional Printing Technology for Patients With Nasal Septal Deformities: A Multicenter Study. JAMA Otolaryngol Head Neck Surg. 2018;144:1145-52.

61. Kim YS, Shin YS, Park DY, Choi JW, Park JK, Kim DH, Kim CH, Park SA. The Application of Three-Dimensional Printing in Animal Model of Augmentation Rhinoplasty. Ann Biomed Eng. 2015;43:2153-62.

62. Park SH, Yun BG, Won JY, Yun WS, Shim JH, Lim MH, Kim DH, Baek SA, Alahmari YD, Jeun JH, Hwang SH, Kim SW. New application of three-dimensional printing biomaterial in nasal reconstruction. Laryngoscope. 2017;127:1036-43.

63. Chiesa-Estomba CM, Aiastui A, González-Fernández I, Hernáez-Moya R, Rodiño C, Delgado A, Garces JP, Paredes-Puente J, Aldazabal J, Altuna X, Izeta A. Three-Dimensional Bioprinting Scaffolding for Nasal Cartilage Defects: A Systematic Review. Tissue Eng Regen Med. 2021;18:343-353.

64. Zhang L, Hu J, Athanasiou KA. The role of tissue engineering in articular cartilage repair and regeneration. Crit Rev Biomed Eng. 2009;37:1–57.

65. Ferril GR, Wudel JM, Winkler AA. Management of complications from alloplastic implants in rhinoplasty. Curr Opin Otolaryngol Head Neck Surg 2013;21:372–378.

66. Glasgold MJ, Kato YP, Christiansen D, Hauge JA, Glasgold AI, Silver FH. Mechanical properties of septal cartilage homografts. Otolaryngol Head Neck Surg 1988;99:374–379.

67. Li X, Cui R, Sun L, Aifantis K, Fan Y, Feng Q, et al. 3D-printed biopolymers for tissue engineering application. Int J Polym Sci 2014;2014:13.

68. Gudmann NS, Karsdal MA. Type II collagen. In: Karsdal MA, ed. Biochemistry of Collagens, Laminins and Elastin. Cambridge, MA: Academic Press; 2016:13-20.

69. Nam JH, Lee SY, Khan G, Park ES. Validation of the optimal scaffold pore size of nasal implants using the 3-dimensional culture technique. Arch Plast Surg. 2020;47:310-316.

70. Trentham DE, Townes AS, Kang AH. Autoimmunity to type II collagen an experimental model of arthritis. J Exp Med. 1977;146:857-868.

71. Yoo TJ, Stuart JM, Takeda T, et al. Induction of Type-Ii collagen autoimmune arthritis and ear disease in monkey. Ann NY Acad Sci. 1986;475:341-342.

72. Lynn AK, Yannas IV, Bonfield W. Antigenicity and immunogenicity of collagen. J Biomed Mater Res B Appl Biomater. 2004;71:343-354.

73. Radhakrishnan S, Nagarajan S, Bechelany M, Kalkura SN. Collagen Based Biomaterials for Tissue Engineering Applications: A Review. Cham: Springer International Publishing; 2020:3-22.

74. Irawan V, Sung TC, Higuchi A, Ikoma T. Collagen scaffolds in cartilage tissue engineering and relevant approaches for future development. Tissue Eng Regen Med. 2018;15:673-697.

75. Shieh SJ, Terada S, Vacanti JP. Tissue engineering auricular reconstruction: in vitro and in vivo studies. Biomaterials. 2004;25:1545-1557.

76. Zeng W, Lin F, Shi T, et al. Fused deposition modelling of an auricle framework for microtia reconstruction based on CT images. Rapid Prototyping Journal. 2008;14:280-284.

77. Liu Y, Zhang L, Zhou G, et al. In vitro engineering of human ear-shaped cartilage assisted with CAD/CAM technology. Biomaterials. 2010;31:2176-2183.

78. Dang, J. M.; Leong, K. W. Natural polymers for gene delivery and tissue engineering. Adv. Drug Delivery Rev. 2006;58: 487−99.

79. Liu M, Zeng X, Ma C, Yi H, Ali Z, Mou X, et al. Injectable hydrogels for cartilage and bone tissue engineering. Bone Res. 2017;5:17014.

80. Wiggenhauser PS, Schantz JT, Rotter N. Cartilage engineering in reconstructive surgery: auricular, nasal and tracheal engineering from a surgical perspective. Regen Med. 2017;12:303–14.

81. Wiggenhauser PS, Schwarz S, Koerber L, Hoffmann TK, Rotter N. Addition of decellularized extracellular matrix of porcine nasal cartilage improves cartilage regenerative capacities of PCL-based scaffolds in vitro. J Mater Sci Mater Med. 2019;30:121.

82. Elsaesser AF, Bermueller C, Schwarz S, Koerber L, Breiter R, Rotter N. In vitro cytotoxicity and in vivo effects of a decellularized xenogeneic collagen scaffold in nasal cartilage repair. Tissue Eng Part A. 2014;20:1668–78.

83. Goldberg-Bockhorn E, Schwarz S, Elsasser A, Seitz A, Korber L, Durselen L et al. Physical characterization of decellularized cartilage matrix for reconstructive rhinosurgery. Laryngorhinootologie. 2014;93:756–63.

84. Schwarz S, Elsaesser AF, Koerber L, Goldberg-Bockhorn E, Seitz AM, Bermueller C et al. Processed xenogenic cartilage as innovative biomatrix for cartilage tissue engineering: effects on chondrocyte differentiation and function. J Tissue Eng Regen Med. 2015;9:E239-51.

85. Schwarz S, Koerber L, Elsaesser AF, Goldberg-Bockhorn E, Seitz AM, Durselen L et al. Decellularized cartilage matrix as a novel biomatrix for cartilage tissue-engineering applications. Tissue Eng Part A. 2012;18:2195–209.

86. Möller T, Amoroso M, Hägg D, Brantsing C, Rotter N, Apelgren P, Lindahl A, Kölby L, Gatenholm P. In Vivo Chondrogenesis in 3D Bioprinted Human Cell-laden Hydrogel Constructs. Plast Reconstr Surg Glob Open. 2017;5:e1227.

87. Guillotin B, Guillemot, F. Cell patterning technologies for organotypic tissue fabrication. Trends Biotechnol. 2011;29:183–190.

88. Frampton JP, Hynd MR, Shuler ML, Shain W. Fabrication and optimization of alginate hydrogel constructs for use in 3D neural cell culture. Biomed Mater. 2011;6:015002.

89. Martinez-vila H, Feldmann EM, Pleumeekers MM, et al. Novel bilayer bacterial nanocellulose scaffold supports neocartilage formation in vitro and in vivo. Biomaterials. 2015;44:122–133.

90. Wu L, Leijten JC, Georgi N, et al. Trophic effects of mesenchymal stem cells increase chondrocyte proliferation and matrix formation. Tissue Eng Part A. 2011;17:1425–1436.

91. Zuo Q, Cui W, Liu F, et al. Co-cultivated mesenchymal stem cells support chondrocytic differentiation of articular chondrocytes. Int Orthop. 2013;37:747–752.

92. Wu L, Prins HJ, Helder MN, et al. Trophic effects of mesenchymal stem cells in chondrocyte co-cultures are independent of culture conditions and cell sources. Tissue Eng Part A. 2012;18:1542–1551.

93. de Windt TS, Hendriks JA, Zhao X, et al. Concise review: unraveling stem cell cocultures in regenerative medicine: which cell interactions steer cartilage regeneration and how? Stem Cells Transl Med. 2014;3:723–733.

94. Leijten JC, Georgi N, Wu L, et al. Cell sources for articular cartilage repair strategies: shifting from monocultures to cocultures. Tissue Eng Part B Rev. 2013;19:31–40.

Bibliografía

Bibliografía